

Real-Space Inversion and Super-Resolution of Ultrafast Scattering using Natural Scattering Kernels

Adi Natan^{1,*}

¹Stanford PULSE Institute, SLAC National Accelerator Laboratory 2575 Sand Hill Road, Menlo Park, CA 94025
(Dated: May 12, 2022)

Directly resolving in real-space multiple atomic motions using ultrafast x-ray or electron scattering is generally limited by the finite detector range. As a result, signal interpretation mostly relies on modeling and simulations of specific excitation pathways. Here, we introduce an approach to resolve ultrafast diffuse scattering signals in real space below the diffraction limit, and recover multiple atomic motions de-novo, using a scattering basis representation that is composed of the measurement parameters and constraints, and the subsequent inversion analysis. We leverage signal priors, such as smoothness and sparsity to deconvolve the spatially transformed signals using convex optimization. We validate the approach on simulated and experimental data, demonstrate super-resolution in real space, and discuss the recovery accuracy and resolution limits vs signal fidelity.

Ultrafast scattering using X-ray free-electron lasers (XFELs) and relativistic electrons are emerging tools to probe motions of photo-excited molecular systems at the angstrom and femtosecond scales. In recent years these methods were successfully used to trace dynamics of molecules in the gas phase [1–11], as well as structural changes of molecules in solution [12–19]. Obtaining the real-space pair distribution function by inversion of the scattering signal was often not possible for these studies because of the limited available range of the scattering vector. As a result, the methods that were developed to interpret the scattering signals were mostly model-based and relied on calculating and attaining trajectory statistics for the specific system under study, where retrieval of the transient structure was usually limited to a single reaction pathway. Complex atomic motions that take place simultaneously and involve multiple pathways were often not resolved or discussed. The inversion of the total measured signal entails an additional complexity, as it can be composed of different types of atom pairs, where each pair contribution has to be disentangled from the overall signal to account for its respective form factors.

Here we introduce a model-free deconvolution approach to overcome the limitations that are imposed by a typical inversion procedure. We show how real-space recovery of multiple and complex motions can be obtained by leveraging the information that naturally arises from the measurement and analysis, including when several types of atom pairs contribute. The approach is applicable for both X-ray and electron scattering, for brevity we'll discuss mostly the former.

X-ray scattering of time-evolving charge densities is generally inelastic, but under typical experimental conditions, the general electronic scattering operator can be replaced with its elastic expression [20, 21]. In experiments, the signal is usually integrated over angle for improved fidelity and subtracted from the signal of the unexcited system, to allow tracing changes of signal positions and

infer dynamics [13]. Considering the isotropic signal part was shown to contain all the nuclear and electronic structural evolution of the charge density [22]. For simplicity, we'll introduce the approach using the isotropic scattering signal, given by the Debye equation [23, 24]:

$$S_0(q, \tau) = \sum_a f_a(q)^2 + \sum_a \sum_{b \neq a} f_a^*(q) f_b(q) 4\pi \int_0^\infty dR R^2 \rho_{a,b}(R, \tau) j_0(qR), \quad (1)$$

where $S_0(q, \tau)$ is the isotropic diffuse scattering signal at time delay τ and at the scattering vector magnitude $q = 4\pi \sin(\theta)/\lambda$, the scattering angle θ and wavelength λ . The double sum is over all atom pairs, $f_i(q)$ is the atomic form factor of the i^{th} atom, $\rho_{a,b}(R, \tau)$ is the pair charge density, and $j_0(qR) = \sin(qR)/qR$ is the zeroth order spherical Bessel function. Direct real-space inversion of Eq. 1 can be done for the case of a single $\rho_{a,b}$ contribution to obtain the isotropic pair density:

$$PD(R, \tau) = \int_0^\infty dq q^2 \frac{S_0(q, \tau) j_0(qR)}{f_a(q) f_b(q)}. \quad (2)$$

The integrand here is often scaled with an exponential function e^{-kq^2} [14, 25] to serve as an effective experimental integration bound, however, this formalism does not capture various aspects of the measurement, such as the experimental configuration, detector truncation, and discretization. As a result, applying Eq. 2 will contain inversion artifacts severely limiting resolution, especially around the few Angstrom length scale that is relevant for molecular structure dynamics.

To illustrate these issues, in Fig 1 we show the inversion of a Dirac delta charge density of a single pair at 2\AA , under typical experimental conditions, limiting the q-range to $0.5 < q < 4\text{\AA}^{-1}$. The inverted waveform in Fig 1d fails to resolve the original delta function position as it is distorted by the finite q-range window and its resolution limit given by $2\pi/4\text{\AA}^{-1} \sim 1.6\text{\AA}$. However, this provides

* natan@stanford.edu

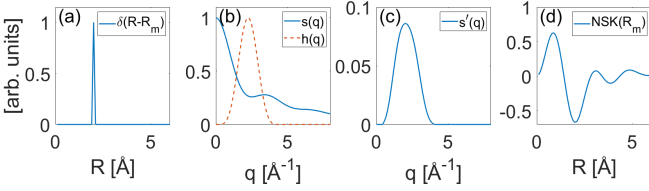


FIG. 1. Formation of a Natural Scattering Kernel (Eq. 3): (a) starting with a Dirac delta pair density in real space, we generate (b) its scattering signal $s(q)$, (c) impose measurement constraints such as a finite q -range represented by $h(q)$, and (d) invert the truncated signal $s'(q)$ to real space.

us with a path to define the Natural Scattering Kernel (NSK) as the function that describes the distortion that a $\delta(R-R_m)$ charge density naturally undergoes in terms of composition, measurement process, and analysis:

$$NSK(R_m) \equiv \mathcal{T}_{q \rightarrow R} \{ \mathcal{M}_{q \rightarrow q} \{ \mathcal{T}_{R \rightarrow q} \{ \delta(R-R_m) \} \} \}. \quad (3)$$

$\mathcal{T}_{\alpha \rightarrow \beta}$ is the transformation from domain α to β , including signal discretization, and \mathcal{M} represents the measurement distortion in q -space. $R_m = m\Delta R$, and ΔR is the sampling resolution with $R_{max} = M\Delta R$. For the isotropic case, the first step is implemented using Eq. 1:

$$\mathcal{T}_{R \rightarrow q} \{ \delta(R - R_m) \} \equiv s(q_i), \quad \{q_i\}_1^{N-1} = \frac{j_{0i}}{j_{0N}} q_{max}. \quad (4)$$

we assume detector discretization dq , an upper bound q_{max} , and resample $s(q)$ at q_i , given by j_{0i} , the i^{th} root of j_0 , with $i=1 \dots N-1$. The distortion due to the measurement can be generally described via:

$$\mathcal{M}_{q \rightarrow q} \{ s(q_i) \} = [s(q_i) * v(q_i)] \cdot h(q_i) + b(q_i) \equiv s'(q_i), \quad (5)$$

Where $v(q) \simeq c_1 q - c_2 q^3 + c_3 q^5$ models the q -varying blur at q_i with coefficients c that are determined by the sample thickness and distance from the detector. $h(q)$ is a window function that represents the detector's finite q -range as well as q -dependent signal absorption, and $b(q)$ is a possible additive background. The transformation back to real-space uses the same discretization scheme:

$$\mathcal{T}_{q \rightarrow R} \{ s'(q_i) \} = \frac{q_{max}^2}{j_{0N}} \sum_{i=1}^{N-1} \mathbf{G}_{m,i} \frac{s'(q_i) q_i}{f_e(q_i)} \equiv NSK(R_m), \quad (6)$$

where $f_e = f_a f_b$, and the transformation matrix:

$$[\mathbf{G}]_{m,i} = 2 \frac{j_0 \left(\frac{j_{0m} j_{0i}}{j_{0N}} \right)}{j_{0N} j_1^2(j_{0i})}. \quad (7)$$

We can now create a set of NSKs along R to form a dictionary \mathcal{D} , an $M \times (N-1)$ matrix that will be used to approximate charge density distributions and explain the

distorted inversion signal under the measurement constraints. The discretization and resampling that are used in Eqs. 4 - 7 were obtained similar to [26, 27], to enable consistent operation rules for multiplication, modulation, and convolution between the R and q domains.

To demonstrate the way NSKs can be used to recover real-space information, we consider a representative case of molecular dynamics under typical experimental conditions. We solved a radial time-dependent Schrodinger equation (TDSE) for diatomic Iodine, with parameters similar to [2], and obtained the time-dependent charge density difference (Fig 2a) exhibiting vibration and dissociation of excited states and depletion of the ground state. We used the calculated charge density to simulate the difference scattering signal $\Delta S_0(q, \tau) = S_0(q, \tau) - S_0(q, 0)$ for each delay τ . We applied typical XFEL scattering geometry, sample distance of 60 mm from an array detector [28], resulting with a q -range $0.5 < q < 4 \text{ \AA}^{-1}$. We assume a signal-to-noise ratio (SNR) of 20 dB, modeled as a q -dependent additive white Gaussian noise, where each q_i bin has sampling statistics proportional to the number of detector pixels contributing to it. We used a Slepian window function [29] for the truncation, and signal resampling of $dq = 0.1 \text{ \AA}^{-1}$ (Fig 2b). We inverted the truncated signal to obtain $PD(R, \tau)$, which is distorted by the measurement constraints and doesn't correctly recover the distances of the TDSE (Fig 2c). We create NSKs with the same measurement constraints, using $R_{max} = 30 \text{ \AA}$, $\Delta R = 0.05 \text{ \AA}$ to form a dictionary \mathcal{D} (Fig 2d) and use it to model the distorted inversion:

$$PD = \mathcal{D}w, \quad (8)$$

Where we seek to estimate the weights vector w to recover the pair density. Naively, one would attempt to solve this model using least-squares minimization: $\min_w \|PD - \mathcal{D}w\|^2$, however, this approach is highly sensitive to noise and is generally unstable numerically when the problem is ill-posed. A standard approach for solving ill-posed inverse problems is to use a regularization framework to promote solutions with properties that are based on the information of the data:

$$\min_w \|PD - \mathcal{D}w\|^2 + \lambda \mathcal{R}(w) \quad (9)$$

Where λ is the regularization parameter that controls the magnitude of the regularization, and the regularizer \mathcal{R} is chosen according to some prior information of the measurement to facilitate solutions with preferable features. A widely used regularization approach that addresses the numerical instabilities and produces low variance solutions is the Tikhonov or ℓ_2 regularization [30], where $\mathcal{R} = \sum |w_i|^2$. Using this regularizer provides the closed-form linear solution: $w = (\mathcal{D}^T \mathcal{D} + \lambda \mathbf{1})^{-1} \mathcal{D}^T PD$ that can be solved using singular value decomposition, where λ can be obtained using the L-curve method [31]

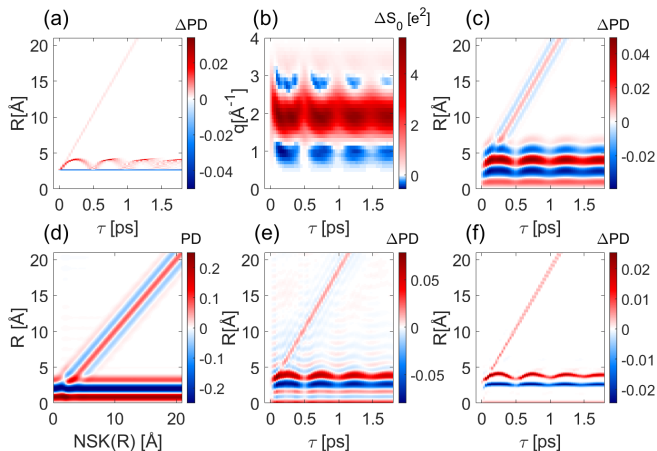


FIG. 2. (a) TDSE calculation of the time-dependent charge density difference (PD normalized to the total charge) for diatomic Iodine resulting in coherent vibration and dissociation wavepacket motions and (b) its simulated difference scattering signal assuming typical experimental conditions (see text). (c) Inverting the truncated signal yields the pair-density difference signal. The limited q -range hinders the ability to recover the positions and motions of the calculated charge density. (d) The NSKs dictionary formed by the measurement constraints is used to deconvolve the distorted pair-density using (e) ℓ_2 and (f) ℓ_1 regularizations (see text).

or by generalized cross-validation [32]. This approach promotes stable and smooth solutions and increases the ability to predict their nature. However, it also often results in most of w elements having non-zero values, as seen in Fig 2e. While this approach handles some of the inversion artifacts, the nature of the solutions it promotes may reduce the ability to resolve weaker signals.

For the case where we assume that the solution for w is sparse, such that the number of sampling points in R that can explain the distorted PD is much smaller than M , the dimension of R , we can use the ℓ_1 regularized least-squares model [33, 34], where $\mathcal{R} = \sum |w_i|$. While this approach doesn't have a closed-form solution, it can be solved using convex optimization. In recent years, several algorithmic approaches have evolved to address this, determine the optimal parameters [35–37], and transforming areas of research such as statistics, machine learning, and signal processing [38–46]. We applied convex optimization for the ℓ_1 regularization case (Eq.9) using CVX, a package for specifying and solving convex programs [47], as seen in Fig 2f. This approach accurately captures real-space information, and enables to super-resolve details such as wavepacket dispersion, while significantly suppressing noise from unrelated distances.

The accuracy of the recovery and the ability to achieve super-resolution depends on the SNR, where we make the distinction between noise originating from an additive source that can be modeled by an appropriate distribution to experimental artifacts that can be characterized and used in the NSK formation (Eq 5). The real-

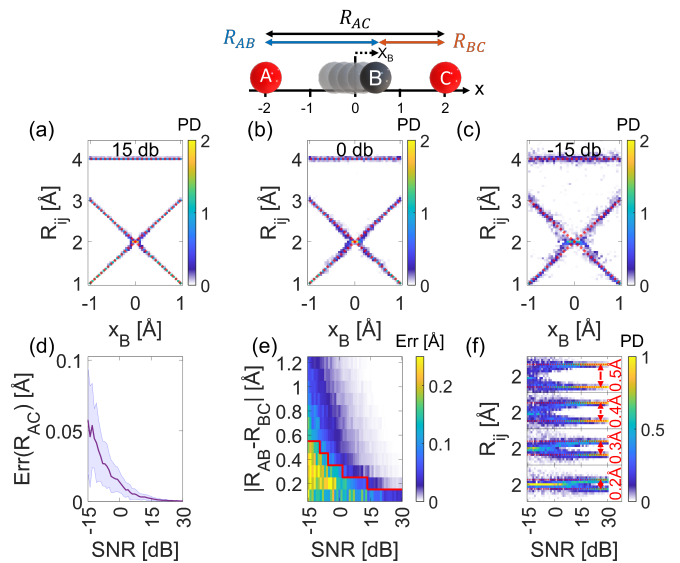


FIG. 3. Recovery accuracy under noise is tested for a 3-atom system, where two pair-distances (R_{AB} , R_{BC}) approach each other below the diffraction limit (top). The scattering is simulated and truncated ($0.5 < q < 4 \text{ \AA}^{-1}$), and inverted using NSKs (ℓ_1 regularization). The inversions for (a) 15, (b) 0, and (c) -15 dB SNRs are shown vs exact distances (dotted red), where PD is normalized by the pair total charge density. The recovery error is proportional to the noise, validating the stability of the approach. (d) For R_{AC} , the average recovery error (solid) and standard deviation (shaded) are $< 0.1 \text{ \AA}$ across SNRs. (e) We use the recovery error for the pair separation $|R_{AB} - R_{BC}|$ to find the minimal resolution both pairs are resolved vs SNR (solid red), (f) determining the super-resolution conditions, with 3.1–7.8 fold enhancement beyond the diffraction limit across SNRs. We obtain that the recovery accuracy in the super-resolution regime is limited by both SNR and pair coalescence.

space resolution is given by the diffraction limit $2\pi/q_{max}$, and super-resolution in the context of diffuse scattering means to resolve two pair-density distances below this limit. To robustly super-resolve using NSKs and ℓ_1 regularization, an additional minimum separation distance between adjacent NSKs is introduced to avoid solution ambiguity below some $\delta R < \nu/q_{max}$, where ν usually depends on signal's properties and fidelity [48–50]. To obtain the minimum separation value we identify two possible cases: when two (or more) pair distances approach each other, and when a pair distance is approaching zero. Because the latter case is not physical, we focus on the recovery accuracy as a function of SNR for the case of coalescence of two distances.

We use a model 3-atom system, similar to CO_2 (Fig 3), where we fix the positions of the outer atoms (A, C) to $x = \pm 2 \text{ \AA}$, while changing the position of (B) the central atom ($-1 \text{ \AA} < x < 1 \text{ \AA}$). When atom B is at $x=0$, the pair-distance R_{AB} will merge with R_{BC} at 2 \AA . We simulate the scattering signal for each of the distances with the same measurement constraints we used for the previ-

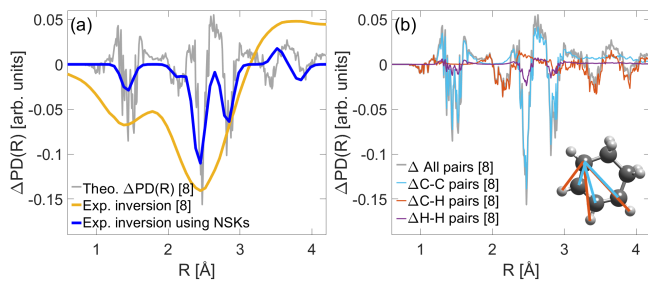


FIG. 4. (a) The theoretical (gray) and experimental (yellow) pair density difference of the photoinduced ring-opening of CHD at 0.55 ps from [8] vs (blue) the inversion and super-resolution of the experimental data using NSKs method presented here. Individual peaks, resolved at $<0.3\text{\AA}$, correspond to atom pair distances which significantly change during the ring-opening. (b) The ab initio simulation highlights the depletion of the C-C (cyan) and C-H (orange) pair distances that are resolved by the NSKs inversion. These distances are illustrated in the CHD steady-state geometry (inset).

ous example $0.5 < q < 4\text{\AA}^{-1}$. We apply the NSK approach and test the recovery for a range of SNRs (-15 to 30 dB), with 20 realizations to each noise level to obtain recovery statistics. We find that the recovery accuracy for the ℓ_1 approach is proportional to the noise level, demonstrating the stability of the approach, and in agreement with theory [48]. For the fixed R_{AC} distance the recovery error is $<0.1\text{\AA}$ across the SNRs (Fig 3d), demonstrating the accuracy of the approach for the case of separated pair distances (Fig 3c). For the case where the two pair distances R_{AB} , R_{BC} approach each other, we obtain a minimal separation of $\delta R \approx 0.35 \pm 0.15\text{\AA}$ and a factor of 3.1–7.8 enhancement over the diffraction limit for the range SNRs used (Fig 3e). We observe that the recovery error in this case is both due to noise and a drift toward the coalescence point (Fig 3f). An additional limiting factor for this analysis is the sparsity assumption. We tested the recovery accuracy as a function of the number of pair distances involved, and obtain the same behavior for the minimal separation condition observed between the two pair distances. Inaccuracies due to this limitation may be addressed by applying an additional real-space blur of the same width to reduce the coalescence artifact effect. For the implementation of this approach for anisotropic signals, see the supplementary material [51].

Extending the approach to experimental data and polyatomic systems with more pair types introduce contributions from different pairs with different form factors, both not separable in the analysis process, as only the total signal $S_0(q)$ is measured. In order to apply the inversion to such cases, we approximate the contributions of different atomic form factors as: $f_e(q) = \sum_{a,b} f_a(q)f_b(q)$, where f_e is an effective form factor of the overall signal $S_0(q)$. Because $f_a(q)f_b(q)$ is a featureless monotonic function in the truncated q -range, its real-space inversion

will mainly contribute to the amplitude of the main lobe found at $0 < R < \pi/q_{max}$. As a result, the inaccuracy using f_e will be limited to an amplitude artifact in that range, which can be neglected as it takes place at pair distances below typical bond lengths. Moreover, this contribution is stationary and doesn't enter signal difference measurements. The outcome will be a pair density distribution where atom-pairs will have an amplitude proportional to their charge densities product, and their detection will be limited by the signal fidelity.

In Fig 4 we apply the NSK inversion approach to an experimental ultrafast electron scattering signal of photoinduced ring-opening of 1,3-cyclohexadiene (CHD), taken from [8]. This well studied polyatomic molecule, has 14 atoms and a total of 91 atom pairs in three groups (C-C, C-H, H-H). We used the effective form factor approximation to invert the experimental signal at 0.55 ps delay, as the structural opening of the ring takes place and 1,3,5-hexatriene (HT) is formed. Our results are in excellent agreement with the ab initio multiple spawning (AIMS) simulations, done at the α -CASSCF(6,4)/6-31G* level of theory, without further processing the trajectories in the same way as the experimental inversion done in [8]. We resolve $<0.3\text{\AA}$ features, including details of several individual pair distances that were not resolved before. We observe the depletion of the initial steady-state C-C distances at 1.4, 2.5, 2.85 \AA , and C-H distance at 2.1 \AA as new distances $>3\text{\AA}$ form due to the ring opening. We obtain a 0.1 \AA shift vs the simulated C-H separation that forms at 3.6 \AA , and a reduced negative peak at 3.3 \AA , that can constrain the temporal HT isomers (cZc, cZt, tZt) contribution discussed in [8].

In summary, we introduce a model-free approach to recover real-space information from ultrafast diffuse scattering signals. Leveraging the measurement limitations with a consistent analysis scheme we form a dictionary of scattering kernels and use it to deconvolve the real space distorted signals. We introduce an effective form factor approximation for polyatomic systems and validate the approach using simulated and experimental scattering data. We demonstrate super-resolution of simultaneous motions de-novo, and discuss the resolution limit as function of fidelity. Future extensions to this approach can be done using different regularization schemes, off-the-grid type methods [52], and inclusion of additional aspects of the scattering process, such as resonant scattering, inelastic and coherent scattering cross terms [21, 53–57]. This approach may help bridging the established pair-distribution function analysis that requires much higher q ranges ($>30\text{\AA}^{-1}$) with time-resolved high-energy 15–25keV diffuse scattering ($q \sim 10\text{\AA}^{-1}$) experiments that are becoming operational in XFELs.

We thank T.J.A. Wolf, D. M. Sanchez, and T. J. Martínez for the experimental data and ab-initio trajectory simulations in [8]. This work was supported by the U.S. Department of Energy, Office of Science, Basic Energy Sciences, Chemical Sciences, Geosciences, and Biosciences Division.

- [1] M. P. Minitti, J. M. Budarz, A. Kirrander, J. S. Robinson, D. Ratner, T. J. Lane, D. Zhu, J. M. Glownia, M. Kozina, H. T. Lemke, M. Sikorski, Y. Feng, S. Nelson, K. Saita, B. Stankus, T. Northey, J. B. Hastings, and P. M. Weber, Imaging molecular motion: Femtosecond x-ray scattering of an electrocyclic chemical reaction, *Phys. Rev. Lett.* **114**, 255501 (2015).
- [2] J. M. Glownia, A. Natan, J. P. Cryan, R. Hartsock, M. Kozina, M. P. Minitti, S. Nelson, J. Robinson, T. Sato, T. van Driel, G. Welch, C. Weninger, D. Zhu, and P. H. Bucksbaum, Self-referenced coherent diffraction x-ray movie of ångström- and femtosecond-scale atomic motion, *Phys. Rev. Lett.* **117**, 153003 (2016).
- [3] B. Stankus, H. Yong, N. Zotev, J. M. Ruddock, D. Bellshaw, T. J. Lane, M. Liang, S. Boutet, S. Carbajo, J. S. Robinson, *et al.*, Ultrafast x-ray scattering reveals vibrational coherence following rydberg excitation, *Nature chemistry* **11**, 716 (2019).
- [4] J. M. Ruddock, N. Zotev, B. Stankus, H. Yong, D. Bellshaw, S. Boutet, T. J. Lane, M. Liang, S. Carbajo, W. Du, *et al.*, Simplicity beneath complexity: counting molecular electrons reveals transients and kinetics of photodissociation reactions, *Angewandte Chemie* **131**, 6437 (2019).
- [5] P. H. Bucksbaum, M. R. Ware, A. Natan, J. P. Cryan, and J. M. Glownia, Characterizing multiphoton excitation using time-resolved x-ray scattering, *Physical Review X* **10**, 011065 (2020).
- [6] A. Natan, A. Schori, G. Owolabi, J. P. Cryan, J. M. Glownia, and P. H. Bucksbaum, Resolving multiphoton processes with high-order anisotropy ultrafast x-ray scattering, *Faraday Discussions* **228**, 123 (2021).
- [7] T. Kierspel, A. Morgan, J. Wiese, T. Mullins, A. Aquila, A. Barty, R. Bean, R. Boll, S. Boutet, P. Bucksbaum, *et al.*, X-ray diffractive imaging of controlled gas-phase molecules: Toward imaging of dynamics in the molecular frame, *The Journal of Chemical Physics* **152**, 084307 (2020).
- [8] T. J. Wolf, D. M. Sanchez, J. Yang, R. Parrish, J. Nunes, M. Centurion, R. Coffee, J. Cryan, M. Gühr, K. Hegazy, *et al.*, The photochemical ring-opening of 1,3-cyclohexadiene imaged by ultrafast electron diffraction, *Nature chemistry* **11**, 504 (2019).
- [9] E. Champenois, D. Sanchez, J. Yang, J. Figueira Nunes, A. Attar, M. Centurion, R. Forbes, M. Gühr, K. Hegazy, F. Ji, *et al.*, Conformer-specific photochemistry imaged in real space and time, *Science* **374**, 178 (2021).
- [10] J. Yang, X. Zhu, J. P. F. Nunes, J. K. Yu, R. M. Parrish, T. J. Wolf, M. Centurion, M. Gühr, R. Li, Y. Liu, *et al.*, Simultaneous observation of nuclear and electronic dynamics by ultrafast electron diffraction, *Science* **368**, 885 (2020).
- [11] Y. Liu, S. L. Horton, J. Yang, J. P. F. Nunes, X. Shen, T. J. A. Wolf, R. Forbes, C. Cheng, B. Moore, M. Centurion, K. Hegazy, R. Li, M.-F. Lin, A. Stolow, P. Hockett, T. Rozgonyi, P. Marquetand, X. Wang, and T. Weinacht, Spectroscopic and structural probing of excited-state molecular dynamics with time-resolved photoelectron spectroscopy and ultrafast electron diffraction, *Phys. Rev. X* **10**, 021016 (2020).
- [12] H. Ihee, Visualizing solution-phase reaction dynamics with time-resolved x-ray liquidography, *Accounts of chemical research* **42**, 356 (2009).
- [13] H. Ihee, M. Wulff, J. Kim, and S.-i. Adachi, Ultrafast x-ray scattering: structural dynamics from diatomic to protein molecules, *International Reviews in Physical Chemistry* **29**, 453 (2010).
- [14] K. H. Kim, J. G. Kim, S. Nozawa, T. Sato, K. Y. Oang, T. W. Kim, H. Ki, J. Jo, S. Park, C. Song, *et al.*, Direct observation of bond formation in solution with femtosecond x-ray scattering, *Nature* **518**, 385 (2015).
- [15] E. Biasin, T. B. van Driel, K. S. Kjær, A. O. Dohn, M. Christensen, T. Harlang, P. Vester, P. Chabera, Y. Liu, J. Uhlig, M. Pápai, Z. Németh, R. Hartsock, W. Liang, J. Zhang, R. Alonso-Mori, M. Chollet, J. M. Glownia, S. Nelson, D. Sokaras, T. A. Assefa, A. Britz, A. Galler, W. Gawelda, C. Bressler, K. J. Gaffney, H. T. Lemke, K. B. Møller, M. M. Nielsen, V. Sundström, G. Vankó, K. Wärnmark, S. E. Canton, and K. Haldrup, Femtosecond x-ray scattering study of ultrafast photoinduced structural dynamics in solvated $[\text{Co}(\text{terpy})_2]^{2+}$, *Phys. Rev. Lett.* **117**, 013002 (2016).
- [16] T. B. Van Driel, K. S. Kjær, R. W. Hartsock, A. O. Dohn, T. Harlang, M. Chollet, M. Christensen, W. Gawelda, N. E. Henriksen, J. G. Kim, *et al.*, Atomistic characterization of the active-site solvation dynamics of a model photocatalyst, *Nature communications* **7**, 1 (2016).
- [17] M. Chollet, R. Alonso-Mori, M. Cammarata, D. Damiani, J. Defever, J. T. Delor, Y. Feng, J. M. Glownia, J. B. Langton, S. Nelson, and *et al.*, The x-ray pump-probe instrument at the linac coherent light source, *Journal of Synchrotron Radiation* **22**, 503–507 (2015).
- [18] K. Haldrup, G. Levi, E. Biasin, P. Vester, M. G. Laursen, F. Beyer, K. S. Kjær, T. Brandt van Driel, T. Harlang, A. O. Dohn, R. J. Hartsock, S. Nelson, J. M. Glownia, H. T. Lemke, M. Christensen, K. J. Gaffney, N. E. Henriksen, K. B. Møller, and M. M. Nielsen, Ultrafast x-ray scattering measurements of coherent structural dynamics on the ground-state potential energy surface of a diplatinum molecule, *Phys. Rev. Lett.* **122**, 063001 (2019).
- [19] M. R. Panman, E. Biasin, O. Berntsson, M. Hermann, S. Niebling, A. J. Hughes, J. Kübel, K. Atkovska, E. Gustavsson, A. Nimmrich, A. O. Dohn, M. Laursen, D. B. Zederkof, A. Honarfar, K. Tono, T. Katayama, S. Owada, T. B. van Driel, K. Kjaer, M. M. Nielsen, J. Davidsson, J. Uhlig, K. Haldrup, J. S. Hub, and S. Westenhoff, Observing the structural evolution in the photodissociation of diiodomethane with femtosecond solution x-ray scattering, *Phys. Rev. Lett.* **125**, 226001 (2020).
- [20] U. Lorenz, K. B. Møller, and N. E. Henriksen, Theory of time-resolved inelastic x-ray diffraction, *Phys. Rev. A* **81**, 023422 (2010).
- [21] M. Simmermacher, N. E. Henriksen, K. B. Møller, A. Moreno Carrascosa, and A. Kirrander, Electronic coherence in ultrafast x-ray scattering from molecular wave packets, *Phys. Rev. Lett.* **122**, 073003 (2019).
- [22] U. Lorenz, K. B. Møller, and N. E. Henriksen, On the interpretation of time-resolved anisotropic diffraction patterns, *New Journal of Physics* **12**, 113022 (2010).
- [23] P. Debye, Zerstreuung von röntgenstrahlen, *Annalen der Physik* **351**, 809 (1915).
- [24] A. O. Dohn, E. Biasin, K. Haldrup, M. M. Nielsen, N. E.

- Henriksen, and K. B. Møller, On the calculation of x-ray scattering signals from pairwise radial distribution functions, *Journal of Physics B: Atomic, Molecular and Optical Physics* **48**, 244010 (2015).
- [25] J. C. Williamson and A. H. Zewail, Ultrafast electron diffraction. 4. molecular structures and coherent dynamics, *The Journal of Physical Chemistry* **98**, 2766 (1994).
- [26] N. Baddour and U. Chouinard, Theory and operational rules for the discrete hankel transform, *J. Opt. Soc. Am. A* **32**, 611 (2015).
- [27] N. Baddour and U. Chouinard, Matlab code for the discrete hankel transform, *Journal of Open Research Software* **5** (2017).
- [28] T. B. Van Driel, S. Nelson, R. Armenta, G. Blaj, S. Boo, S. Boutet, D. Doering, A. Dragone, P. Hart, G. Haller, *et al.*, The epix10k 2-megapixel hard x-ray detector at lcls, *Journal of synchrotron radiation* **27** (2020).
- [29] D. Slepian, Prolate spheroidal wave functions, fourier analysis, and uncertainty—v: The discrete case, *Bell System Technical Journal* **57**, 1371 (1978).
- [30] G. H. Golub, P. C. Hansen, and D. P. O’Leary, Tikhonov regularization and total least squares, *SIAM journal on matrix analysis and applications* **21**, 185 (1999).
- [31] P. C. Hansen and D. P. O’Leary, The use of the l-curve in the regularization of discrete ill-posed problems, *SIAM journal on scientific computing* **14**, 1487 (1993).
- [32] P. C. Hansen, *Rank-deficient and discrete ill-posed problems: numerical aspects of linear inversion* (SIAM, 1998).
- [33] S. Chen and D. Donoho, Basis pursuit, in *Proceedings of 1994 28th Asilomar Conference on Signals, Systems and Computers*, Vol. 1 (IEEE, 1994) pp. 41–44.
- [34] R. Tibshirani, Regression shrinkage and selection via the lasso, *Journal of the Royal Statistical Society: Series B (Methodological)* **58**, 267 (1996).
- [35] S. Boyd, N. Parikh, and E. Chu, *Distributed optimization and statistical learning via the alternating direction method of multipliers* (Now Publishers Inc, 2011).
- [36] N. Parikh and S. Boyd, Proximal algorithms, *Foundations and Trends in optimization* **1**, 127 (2014).
- [37] E. Candes and J. Romberg, l1-magic: Recovery of sparse signals via convex programming, URL: www.acm.caltech.edu/l1magic/downloads/l1magic.pdf **4**, 14 (2005).
- [38] H. Lee, A. Battle, R. Raina, and A. Y. Ng, Efficient sparse coding algorithms, in *Advances in neural information processing systems* (Citeseer, 2007) pp. 801–808.
- [39] J. Mairal, F. Bach, J. Ponce, and G. Sapiro, Online dictionary learning for sparse coding, in *Proceedings of the 26th annual international conference on machine learning* (2009) pp. 689–696.
- [40] K. Gregor and Y. LeCun, Learning fast approximations of sparse coding, in *Proceedings of the 27th international conference on international conference on machine learning* (2010) pp. 399–406.
- [41] D. L. Donoho, Compressed sensing, *IEEE Transactions on information theory* **52**, 1289 (2006).
- [42] E. J. Candès, J. Romberg, and T. Tao, Robust uncertainty principles: Exact signal reconstruction from highly incomplete frequency information, *IEEE Transactions on information theory* **52**, 489 (2006).
- [43] M. Lustig, D. Donoho, and J. M. Pauly, Sparse mri: The application of compressed sensing for rapid mr imaging, *Magnetic Resonance in Medicine: An Official Journal of the International Society for Magnetic Resonance in Medicine* **58**, 1182 (2007).
- [44] M. F. Duarte, M. A. Davenport, D. Takhar, J. N. Laska, T. Sun, K. F. Kelly, and R. G. Baraniuk, Single-pixel imaging via compressive sampling, *IEEE signal processing magazine* **25**, 83 (2008).
- [45] O. Katz, Y. Bromberg, and Y. Silberberg, Compressive ghost imaging, *Applied Physics Letters* **95**, 131110 (2009).
- [46] T. Driver, S. Li, E. G. Champenois, J. Duris, D. Ratner, T. J. Lane, P. Rosenberger, A. Al-Haddad, V. Averbukh, T. Barnard, *et al.*, Attosecond transient absorption spooktscopy: a ghost imaging approach to ultrafast absorption spectroscopy, *Physical Chemistry Chemical Physics* **22**, 2704 (2020).
- [47] M. Grant and S. Boyd, Cvx: Matlab software for disciplined convex programming, version 2.1 (2014).
- [48] E. J. Candès and C. Fernandez-Granda, Super-resolution from noisy data, *Journal of Fourier Analysis and Applications* **19**, 1229 (2013).
- [49] C. Fernandez-Granda, Super-resolution of point sources via convex programming, *Information and Inference: A Journal of the IMA* **5**, 251 (2016).
- [50] V. Duval and G. Peyré, Exact support recovery for sparse spikes deconvolution, *Foundations of Computational Mathematics* **15**, 1315 (2015).
- [51] See Supplemental Material at [URL will be inserted by publisher] for the implementation of the NSKs approach to general anisotropic scattering signals.
- [52] P. Catala, V. Duval, and G. Peyré, A low-rank approach to off-the-grid sparse superresolution, *SIAM Journal on Imaging Sciences* **12**, 1464 (2019).
- [53] G. Dixit, O. Vendrell, and R. Santra, Imaging electronic quantum motion with light, *Proceedings of the National Academy of Sciences* **109**, 11636–11640 (2012).
- [54] D. Popova-Gorelova and R. Santra, Imaging interatomic electron current in crystals with ultrafast resonant x-ray scattering, *Physical Review B* **92**, 184304 (2015).
- [55] D. Popova-Gorelova, D. A. Reis, and R. Santra, Theory of x-ray scattering from laser-driven electronic systems, *Physical Review B* **98**, 224302 (2018).
- [56] M. Simmermacher, A. Moreno Carrascosa, N. E. Henriksen, K. B. Møller, and A. Kirrander, Theory of ultrafast x-ray scattering by molecules in the gas phase, *The Journal of chemical physics* **151**, 174302 (2019).
- [57] G. Hermann, V. Pohl, G. Dixit, and J. C. Tremblay, Probing electronic fluxes via time-resolved x-ray scattering, *Physical Review Letters* **124**, 013002 (2020).